

# Computations underlying *Drosophila* photo-taxis, odor-taxis, and multi-sensory integration

Ruben Gepner<sup>1,2</sup>, Mirna Mihovilovic Skanata<sup>1,2</sup>, Natalie M. Bernat<sup>1</sup>, Margarita Kaplow<sup>3</sup>, and Marc Gershow<sup>1</sup>

## Abstract

To better understand how organisms make decisions on the basis of temporally varying multi-sensory input, we identified computations made by *Drosophila* larvae responding to visual and optogenetically induced fictive olfactory stimuli. We modeled the larva's navigational decision to initiate turns as the output of a Linear-Nonlinear-Poisson cascade. We used reverse-correlation to fit parameters to this model; the parameterized model predicted larvae's responses to novel stimulus patterns. For multi-modal inputs, we found that larvae linearly combine olfactory and visual signals upstream of the decision to turn. We verified this prediction by measuring larvae's responses to coordinated changes in odor and light. We studied other navigational decisions and found that larvae integrated odor and light according to the same rule in all cases. These results suggest that photo-taxis and odor-taxis are mediated by a shared computational pathway.

## Introduction

Many small organisms navigate their environments by decoding temporal variation in receptor activity to bias motor output decisions (Albrecht and Bargmann, 2011; Berg and Brown, 1972; Fishilevich et al., 2005; Gershow et al., 2012; Gomez-Marin et al., 2011; Kane et al., 2013; Lockery, 2011; Louis et al., 2008; Luo et al., 2008; Luo et al., 2010; Pierce-Shimomura et al., 1999; Ryu and Samuel, 2002; Sawin et al., 1994). The dynamics of these organisms' decision-making are intimately linked to the properties of the underlying chemical or neural substrates (Asahina et al., 2009; Bretscher et al., 2011; Busch et al.,

---

<sup>1</sup> Dept. of Physics, New York University, New York, NY

<sup>2</sup> These authors contributed equally to this work.

<sup>3</sup> Center for Neural Science, New York University, New York, NY

2012; Chronis et al., 2007; Clark et al., 2007; Emonet and Cluzel, 2008; Kato et al., 2014; Korobkova et al., 2004; Luo et al., 2014; Miller et al., 2005; Segall et al., 1986; Shimizu et al., 2010; Suzuki et al., 2008). In their natural environments, animals are confronted by variable and frequently conflicting input arriving via multiple sensory pathways. How these simple organisms respond to multi-modal stimuli and how their neural circuits integrate and prioritize multi-sensory information remains unknown.

We sought to decode the computations underlying the *Drosophila* larva's response to visual and olfactory cues, when presented individually or in combination. The second instar larva uses a similar strategy for navigating environments with spatially varying odor concentrations, light, and heat. Larvae move forward in a series of relatively straight *runs* interspersed with reorienting *turns*, and increase the frequency and magnitude of their turns in response to unfavorable changes in the stimulus (Busto et al., 1999; Gershow et al., 2012; Gomez-Marin et al., 2011; Kane et al., 2013; Klein et al., 2014; Louis et al., 2008; Luo et al., 2010; Sawin et al., 1994; Scantlebury et al., 2007). During turns, larvae survey the local environment using side-to-side head sweeps to determine the direction of the next run (Gershow et al., 2012; Gomez-Marin et al., 2011; Kane et al., 2013; Klein et al., 2014; Luo et al., 2010; Sawin et al., 1994). That the larva uses the same strategy to respond to a variety of stimuli suggests navigation may be mediated by a single circuit that combines input from the various sensory organs. Alternately, this apparent commonality might result from the larva's limited repertoire of motor outputs with which to implement a navigational response. Perhaps independent circuits mediate the "decision" portion of each navigational algorithm and only converge at the motor output level (Frye and Dickinson, 2004).

We sought a computational model that could describe the transformation from sensory input to navigational decisions for uni- and multi- modal stimuli and that could differentiate between shared and parallel navigational circuits. The Linear-Nonlinear-Poisson (LNP) model (Bialek and van Steveninck, 2005; Chichilnisky, 2001; Dayan, 2001; Kim et al., 2011; Ringach and Shapley, 2004; Schwartz et al., 2006) is

widely used to relate time-varying input to stochastic output. In this model, decisions (e.g. to initiate a turn, **Fig 1A-B**) are generated according to a Poisson process whose underlying rate at time  $t$  is:

$$r(t) = f((A * S)(t)); (A * S)(t) = \int_0^\infty A(\tau)S(t - \tau)d\tau$$

where  $S(t)$  is the input signal,  $A$  is a linear filter, and  $f$  is a nonlinear function (**Fig 1B**). Thus for uni-modal inputs, we aimed to develop models of the form:

$$r_o(t) = f(x_o(t)) \text{ (odor)}$$

$$r_l(t) = g(x_l(t)) \text{ (light)}$$

where  $x_o(t) = (A_o * S_o)(t)$  and  $x_l(t) = (A_l * S_l)(t)$  are the outputs of the linear filters for odor and for light respectively. For multi-modal input, we sought either a model in which turns are initiated independently by separate circuits

$$r_{o-l}(t) = f(x_o(t)) + g(x_l(t)) \text{ (independent pathways)}$$

or one in which odor and light information are combined more generally

$$r_{o-l}(t) = h(x_o(t), x_l(t)) \text{ (nonlinear integration)}$$

## Results

We began by exploring larvae's responses to uni-modal stimuli. *Drosophila* larvae avoid light and carbon dioxide and are attracted to Ethyl Acetate (EtAc). The sensory input pathways are well-characterized for each of these stimuli. The larva's navigational response to light is mediated primarily by four photoreceptor neurons in each of two primitive eye-spots (Hassan et al., 2005; Kane et al., 2013; Keene et al., 2011; Keene and Sprecher, 2012; Sprecher and Desplan, 2008). A single pair of Gr21a expressing receptor neurons mediates the larva's CO<sub>2</sub> response (Faucher, 2006; Jones et al., 2007; Kwon et al., 2007; Python and Stocker, 2002). Or42a and Or42b are the primary EtAc olfactory receptors (Asahina et al., 2009; Kreher et al., 2005; Kreher et al., 2008), and larvae are capable of decoding odor gradients on the basis of only Or42a or Or42b receptor neurons (Asahina et al., 2009; Louis et al., 2008).

Larvae initiate turns in response to increasing light intensities (Hassan et al., 2005; Kane et al., 2013; Sawin et al., 1994; Scantlebury et al., 2007) and carbon dioxide concentrations (Gershow et al., 2012) and decreasing EtAc concentrations (Gershow et al., 2012; Gomez-Marin et al., 2011). To investigate the larva's decision to turn in response to visual cues, we presented 448 nm blue light to wild-type larvae. To probe olfactory computations, we expressed *UAS-CsChrimson* (Klapoetke et al., 2014), a red light activable cation channel, in Gr21a, Or42a, and Or42b receptor neuron pairs. We used 655 nm red light (outside the sensitive range of the larva's visual pigments (Salcedo et al., 1999)) to activate these neurons and presented a constant dim blue light background (Klapoetke et al., 2014) to mask any visual response to the red light.

We presented groups of larvae with fluctuating levels of red or blue light and analyzed their resulting behaviors using machine vision software (Gershow et al., 2012) to identify each navigational decision (**Fig 1C-1**). We determined the parameters of the LNP model by measuring the reverse-correlation (Bialek and van Steveninck, 2005; Chichilnisky, 2001; Dayan, 2001; Kim et al., 2011; Klein et al., 2014; Ringach and Shapley, 2004; Schwartz et al., 2006; Westwick et al., 2003) between the stimulus and evoked behaviors (**Fig 1C**).

For light, odor, and carbon dioxide, the derivative of stimulus intensity is more salient to larvae than the stimulus value itself (Gershow et al., 2012; Gomez-Marin and Louis, 2014; Gomez-Marin et al., 2011; Kane et al., 2013). Typically in reverse-correlation experiments, rapidly changing uncorrelated stimulus intensities are provided (generated e.g. by choosing random binary values, random normally distributed values, or values from an M-sequence). Because of regression to the mean, these sequences have derivatives that are correlated on time scales longer than the update period. Thus, if we provided uncorrelated stimulus intensities and larvae turned in response to an increase in light, we would expect an average decrease in light after turns. This would complicate analyses of decisions, like whether to accept or reject a head sweep, the larva makes following a turn. We therefore chose a stimulus optimized for

analysis of the larva's response to derivatives, a Brownian random walk, whose derivatives (on all time scales) are independent identically distributed Gaussian variables.

First, we computed the turn-triggered average (TTA) of the light intensity derivatives (**Fig 2A**). We found: wild-type larvae turn in response to an increase in blue light but were unresponsive to red light masked by dim blue light (even when fed all-trans-retinal); larvae expressing CsChrimson in EtAc sensing neurons (*Or42a>CsChrimson*, *Or42b>CsChrimson*) turned in response to a *decrease* in red light; and larvae expressing CsChrimson in the CO<sub>2</sub> receptor (*Gr21a>CsChrimson*) turned in response to an *increase* in red light. These results match the larva's strategies for navigating static gradients of natural stimuli; turning in response to increases in light, decreases in EtAc, and increases in CO<sub>2</sub>. In all cases (excepting the wild-type red-light control), larvae considered changes over the previous ~2.5 seconds when deciding to turn, and derivatives were maximally salient about 0.6-0.8 seconds before a turn was actually initiated.

For each set of reverse-correlation experiments, we used the TTA as the convolution kernel to calculate the linear filter outputs and computed the turn rate as a nonlinear function of the filter output (**Fig 2B**). To test the predictive power of the LNP model, we presented larvae with light intensity square waves. We compared the resulting turn rates to those predicted by our LNP model fits (**Fig 2C**). The cyan lines in **Fig 2C** show the exact predictions of the model, with no free parameters. We found that in all cases, except for *Gr21a>CsChrimson*, the step response has a longer duration than predicted by the LNP model, and there is an unpredicted sustained decrease in turn rate following a favorable change (at  $t = 0$ ), but given the inherent variability of behavior and the simplicity of the LNP model, the reverse-correlation experiments predicted the temporal course of the larva's response to step changes surprisingly well.

We were concerned that over the course of the 20 minute behavioral experiments, continuous exposure to red light might exhaust the ability of CsChrimson to excite neural activity or that larvae

might adapt to the stimulus presentation and cease responding. To test whether this was the case, we separately analyzed the first and second ten minutes of the experiments (**Fig 2 – figure supplement 1**). In all cases, we recovered the same turn-triggered average (**Fig 2 – figure supplement 1,A**) using data from only the first ten minutes, only the second ten minutes, or the entire data set. We found that for visual and attractive odor inputs, the slope of the nonlinear function was steeper (**Fig 2 – figure supplement 1,B**) in the first ten minutes than in the second ten, indicating larvae were slightly less responsive to stimulus changes in the latter half of the experiments. For fictive CO<sub>2</sub>, on the other hand, we found that larvae were actually more responsive in the second ten minutes, representing sensitization rather than adaptation. In all cases, the results for the two halves of the experiments were similar enough to justify using all 20 minutes of data in our analyses. To test the self-consistency of our model, we used the parameters extracted from the first ten minutes of experiments to predict the larva's turning rate in the second ten minutes (**Fig 2 – figure supplement 1,C**). We found excellent agreement between predictions and measurements at lower turn rates. At higher turn rates, we found that in the second ten minutes, larvae turned less than predicted for light and attractive odor cues and more than predicted for CO<sub>2</sub> cues, again reflecting modest adaptation and sensitization.

Next we explored how larvae bias the size and directions of turns. Larvae make larger turns when subject to unfavorably changing conditions (Gershow et al., 2012; Kane et al., 2013; Luo et al., 2010), so we calculated the TTA for large and small turns separately (**Fig 2D**). For approximately 10-15 seconds prior to the start of large turns, there was an average gradual increase in blue light levels for visual experiments, and an average gradual decrease in red light levels for *Or42a>CsChrimson* and *Or42b>CsChrimson* experiments. Over the same time period, for small turns, there was a slight average decrease in blue light and increase in red light. Interestingly, immediately prior to the initiation of a turn, the average change in stimulus was the same for large and small turns. Thus larvae consider the change in light intensity and attractive odor concentration over the previous 10-15 seconds when deciding the

size of their turns, but the size of the stimulus change that leads the larva to actually initiate a turn appears not to influence turn size. In contrast, for *Gr21a>CsChrimson* larvae, the size of a turn was determined by the magnitude of the increase immediately preceding a turn.

After initiating turns, larvae use head-sweeps as probes to find a favorable direction for the next run (Gershow et al., 2012; Gomez-Marin and Louis, 2014; Gomez-Marin et al., 2011; Kane et al., 2013; Klein et al., 2014; Luo et al., 2010). Head-sweeps in favorable directions are more likely to be accepted, beginning a new run in that direction. Head-sweeps in unfavorable directions are more likely to be rejected, resulting in one or more additional head-sweeps. To characterize the larva's decision to accept or reject a head-sweep, we measured the head-sweep triggered average, aligned to the start of a head-sweep, separately for rejected and accepted head-sweeps (**Fig 2E**). All head-sweep triggered averages show a large change immediately before the start of the head-sweep; this is the stimulus change that triggered the larva's decision to turn. We found that during accepted head-sweeps, average blue light levels and *Gr21a* activity decreased and *Or42a* and *Or42b* activity increased, all favorable changes. During rejected head-sweeps, the reverse was true: average blue light and *Gr21a* activity levels increased and *Or42a* and *Or42b* activity decreased. Surprisingly, for *Gr21a>CsChrimson* larvae, larger increases in activity prior to the head-sweep start led to an increased probability of rejecting the head-sweep.

Our uni-modal experiments showed *CsChrimson* induced activity in olfactory neurons evokes navigational behaviors, and reverse correlation can be used to identify both visual and olfactory computations. We also found that activity in  $\text{CO}_2$  receptor neurons is interpreted according to different rules than for light or attractive odors.

We next asked how the larva integrates visual and olfactory information when making navigational decisions. We carried out reverse-correlation experiments with simultaneous uncorrelated light and attractive odor stimuli, using dim blue light to activate the visual system and intense red light to activate

CsChrimson expressed in *Or42a* receptor neurons. We found the TTA for both signals (**Fig. 3A**), and we applied the resulting filters to our input signals to find  $x_o(t)$  and  $x_L(t)$ , the outputs of the linear odor and light filters, at each point in time. We scaled the filters so that  $x_o(t)$  and  $x_L(t)$  had unit variance in the stimulus ensemble (Pillow and Simoncelli, 2006). To determine whether the larva's turning decisions result from independent olfactory and visual pathways, we examined the statistics of the *turn-triggered ensemble* (**Fig. 3B**). In our white noise experiments,  $x_o(t)$  and  $x_L(t)$  are independent Gaussian variables with mean 0, so it can be shown (Bialek and van Steveninck, 2005)

$$E[x_o x_L | \text{turn}] = E[\partial^2 r_{o-L}(t) / \partial x_o \partial x_L]$$

In general, this value will be nonzero, but in the independent pathways model (**Fig 3C, Fig 3 – figure supplement 1**), the mixed partial derivative is identically 0, so

$$E[x_o x_L | \text{turn}] = 0 \text{ (independent pathways)}$$

In fact, we found  $\langle x_o x_L | \text{turn} \rangle = 0.23$ , disfavoring the independent pathways hypothesis.

If larvae integrate odor and light information when making turning decisions, what form does this integration take? A potentially favorable (Angelaki et al., 2009; Ma et al., 2006) approach would be for the larva to use a simple linear combination of uni-modal filter outputs as the basis for downstream multi-modal processing (**Fig 3 – figure supplement 2**). In this case, the turn rate would be given by

$$r_{o-L} = h(\cos \theta x_o(t) + \sin \theta x_L(t)) \text{ (early linear combination)}$$

Here  $\theta$  is a constant reflecting the relative importance of each filter output to the computation ( $\theta = 0$  would mean larvae respond only to odor and  $\theta = 90^\circ$  would mean larvae respond only to light).

We used both the independent pathways and early linear combination models to predict the turn-triggered probability density of  $(x_o, x_L)$  and found better agreement between the data and the early linear combination prediction (**Fig 3D**) than the independent pathways predictions (**Fig 3C**).



In the early linear combination model, the turn rate is a function of a 1-dimensional stimulus vector –  $\cos \theta x_O(t) + \sin \theta x_L(t)$  – so a rotation of odor-light convolution space (**Fig 3E**)

$$\begin{pmatrix} u(t) \\ v(t) \end{pmatrix} = \begin{pmatrix} \cos \theta & \sin \theta \\ -\sin \theta & \cos \theta \end{pmatrix} \begin{pmatrix} x_O(t) \\ x_L(t) \end{pmatrix}$$

should produce a single parameter,  $u$ , that carries as much information about turn decisions as the pair  $(x_O, x_L)$  together, and an orthogonal parameter,  $v$ , that carries no information at all. The Kullback-Leibler divergence between the stimulus and turn-triggered distributions describes the amount of information stimulus parameters carry about the decision to initiate a turn (Pillow and Simoncelli, 2006); we calculated this divergence for the pair  $(x_O, x_L)$  and for  $x_O, x_L, u$ , and  $v$  individually (**Fig 3B**) and found that  $u$  alone is as nearly as informative as both  $x_O$  and  $x_L$  and that  $v$  contributes very little to the decision to turn, further supporting the early linear combination model.

Can the observed summation of visual and odor inputs be explained by blue light activation of the CsChrimson channel? To probe for cross-talk between visual and olfactory channels, we repeated the multi-sensory experiments (again presenting both red and blue stimuli simultaneously) using genetically blind larvae expressing CsChrimson in *Or42a* neurons and using wild-type larvae not expressing CsChrimson (**Fig 3 – figure supplement 3**). Blind larvae responded only to red light (**Fig 3 – figure supplement 3,B**) while larvae not expressing CsChrimson responded only to blue light (**Fig 3 – figure supplement 3,C**).

To further compare the independent pathways and early linear combination models, we measured larvae's responses to simultaneous step changes in *Or42a* receptor neuron activity and blue light (**Fig 4**). We presented larvae with all possible combinations of favorable, neutral, and unfavorable steps of red light (fictive odor) and blue light (visual cue). We used the kernels calculated from the reverse-correlation experiments and fit the nonlinear functions parameterizing the early linear combination and independent pathways models to the observed turn rates. We found that despite having fewer free fit

parameters, the early linear combination model (magenta line, **Fig 4**) better predicted the response to conflicting and aligned multi-sensory input than the independent pathways model (cyan line, **Fig 4**).

For changes in only light or only odor, larvae increase their turn rates significantly more for unfavorable changes (panels **ii** and **iii**) than they decrease their turning in response to favorable changes (**i** and **vi**). Thus the independent pathways model, which sums separate rates for light and odor changes, predicts that in response to conflicting favorable and unfavorable changes (**iv** and **viii**), the larvae will still significantly increase their turning. Instead, conflicting changes in odor and light cancel each other out, as predicted by the early linear combination model. That larvae turn in response to increases in blue light (**iii**, **v**) but decreases in red light (**ii**, **v**) further confirms that the two light sources are activating different sensory pathways. For instance, if blue light were primarily activating CsChrimson, we would expect that decreasing blue and red light together (**viii**) would provoke more turning than decreasing red light alone (**ii**), but in fact *increasing* blue light while *decreasing* red light (**v**) provokes the largest increase in turning.

We wondered whether the larva might use the same linear combination of light and odor signals to make other navigational decisions, like whether to accept or reject head-sweeps. Although we previously determined a maximally informative combination of *filtered* odor and light inputs, the convolution kernels have similar shapes, so we might reasonably use the same rules to combine the raw input stimuli.

$$\begin{pmatrix} \mu(t) \\ \nu(t) \end{pmatrix} = \begin{pmatrix} \cos \theta & \sin \theta \\ -\sin \theta & \cos \theta \end{pmatrix} \begin{pmatrix} O(t) \\ L(t) \end{pmatrix}; O(t) = -\frac{dI_{red}}{dt}/I_r^0; L(t) = \frac{dI_{blue}}{dt}/I_b^0$$

Here  $I_r^0$  and  $I_b^0$  are the normalization factors required to make the convolution kernels have unit variance, and  $\theta$  was determined as a parameter of the early linear combination LNP model (**Fig 3D**). We carried out reverse correlation analysis on these rotated coordinates. We found: the turn triggered average of  $\nu(t)$  was nearly 0 (**Fig 5A**); the size-sorted TTA of  $\nu(t)$  was nearly 0 and the same for both small and large turns (**Fig 5B**); and the head-sweep triggered average of  $\nu(t)$  was nearly 0 and the same

for accepted and rejected head-sweeps (**Fig 5C**). Thus larvae used a single linear combination of odor and light -  $\mu(t)$  - to determine whether to turn, how large of a turn to make, and whether to reject or accept head-sweeps, strongly suggesting odor and light inputs are combined at early stages of the navigational circuitry.

Finally, we asked whether the larva might shift its attention between stimulus inputs. For instance, if a larva initiates a turn due to an increase in light, might it prioritize light changes over odor changes in deciding whether or not to accept the turn's first head-sweep? To test this, we re-examined the head-sweep acceptances and rejections from the multi-stimulus white noise experiments, sorting them based on the favorability of light and odor changes preceding the turn start (**Fig 6A**). For instance, in quadrant II, larvae turned following a recent favorable odor change and unfavorable light change. If an unfavorable light change caused otherwise neutral larvae to attend more strongly to light, we would expect that following a quadrant II turn, larvae would be more attentive to light changes than average. Alternately, if some larvae in the population were already attending to light more strongly than odor, we would expect them to be over-represented in the group of larvae turning in response to unfavorable changes in light coupled with favorable changes in odor. Thus we would again expect that following a quadrant II turn, larvae would be attending more strongly to light than in the average population. Similarly, following quadrant IV turns, we would expect larvae to be attending more strongly to odor.

To measure the importance of light and odor changes during head sweeps, we subtracted the average derivative of light level during accepted head sweeps from the average derivative of light level during rejected head sweeps (**Fig 6B**). Regardless of which stimulus likely triggered the decision to turn, for both light and odor, we found the same differences between accepted and rejected head-sweeps. Thus we found no evidence that the larva modulated the relative importance of light or odor changes when deciding whether to accept or reject a head-sweep. Indeed, for all combinations of light and odor

changes preceding a turn, the same linear combination of odor and light inputs appeared to be equally salient in deciding whether to accept or reject a head-sweep (**Fig 6C**).

## **Discussion**

A key step in “cracking” neural circuits is defining the computations carried out by those circuits (Clark et al., 2013; Olsen and Wilson, 2008). Recent work has refined the measurements of circuits’ behavioral outputs, e.g. from simply counting animals accumulating near an odor source (Monte et al., 1989) to specifying the sequence of motor outputs that allow odor gradient ascent (Gershow et al., 2012; Gomez-Marin and Louis, 2014; Gomez-Marin et al., 2011). Here we carried on this refinement, quantifying the transformation from sensory activity to motor decision with sub-second temporal resolution. Our reverse-correlation analysis captured the essential features of the larva’s navigational decision making, including the time scales and stimulus features associated with various decisions (**Fig 2**).

Our results are consistent with the understanding of how larvae navigate natural environments previously developed by observing behavior in structured environments of light or gaseous odors. For instance, when placed in environments with spatially varying Ethyl Butyrate (Gomez-Marin and Louis, 2014; Gomez-Marin et al., 2011) or Ethyl Acetate (Gershow et al., 2012) concentrations, larvae initiate turns more frequently when headed in directions of decreasing concentrations of these attractive odors. In this work, we showed that larvae initiate turns in response to a decrease in activity in Or42a or Or42b receptor neurons, the primary receptors for Ethyl Acetate and Ethyl Butyrate. Additionally, we showed that larvae mainly use only the previous two seconds of receptor activity to decide whether to turn (**Fig 2A**). This detail cannot be resolved from experiments in natural odor gradients, nor can the fact that larvae integrate changes in odor receptor activity over a much longer time period to decide the size of their turns (**Fig 2D**).

When larvae move their heads through a spatially heterogeneous environment, they generate changes in sensory input that could be used to decode local spatial gradients. It has been directly shown that warming a cold larva during a head-sweep causes the larva to accept that head-sweep, beginning a new run (Luo et al., 2010). For light and odor, a strong circumstantial case has been made that larvae use information gathered during head-sweeps to bias turn direction: the first head-sweep of a turn is unbiased (Gershow et al., 2012; Kane et al., 2013) but larvae are more likely to begin a run following a sweep in a direction of higher concentration of attractive odor, lower concentration of carbon dioxide, or lower luminosity (Gershow et al., 2012; Gomez-Marin and Louis, 2014; Gomez-Marin et al., 2011; Kane et al., 2013) and larvae with only a single functional odor receptor can still bias turn direction via head-sweeping (Gomez-Marin and Louis, 2014). In this work we directly show that larvae do in fact use changes in odor receptor activity and light level measured during head-sweeps to determine whether to begin a new run or initiate a second head-sweep (**Fig 2E**).

Our experiments with a single stimulus also found a previously unknown difference in how larvae use CO<sub>2</sub> receptor activity to modulate turn size and head-sweep acceptance compared to visual stimuli and to attractive olfactory receptor activity (**Fig 2D,E**). This could be related to a difference we previously observed in how larvae modulate their forward motion in response to changes in CO<sub>2</sub> concentration compared to changes in light intensity or EtAc concentration. In previous work, we measured larvae's responses to linear temporal ramps of light intensity (Kane et al., 2013), and EtAc and CO<sub>2</sub> concentrations (Gershow et al., 2012). For light and EtAc, we found that larvae changed their rate of turning and the size of their turns in response to changing environmental conditions, but when they were actually engaged in forward movement, their speed of progress was the same whether conditions were improving or declining. In contrast, we found that larvae dramatically decreased their forward run speed in response to increases in the concentration of CO<sub>2</sub>. Larvae with non-functional CO<sub>2</sub> receptors did

not change their speed at all in response to CO<sub>2</sub>, so this modulation was due to a sensory-motor transformation and not to metabolic effects.

Larvae move forward through a series of tail to head peristaltic waves of muscle contraction (Heckscher et al., 2012; Lahiri et al., 2011) and modulate their forward speed by changing the frequency with which they initiate these waves (Heckscher et al., 2012). The observed CO<sub>2</sub> dependent speed modulation might therefore reflect the presence of a pathway by which Gr21a receptor neuron activity can down-regulate the probability of initiating forward peristaltic waves. In order to accept a head-sweep, i.e. transition from head-sweeping to forward movement, larvae must initiate a new peristaltic wave (Lahiri et al., 2011). If an increase in Gr21a activity decreases the probability of initiating such a wave, this would explain why an increase in Gr21a activity *prior* to head-sweep initiation results in an increased probability of head-sweep rejection (**Fig 2E**). Similarly, an increase in Gr21a activity might bias the larva towards larger reorientations (**Fig 2D**) by decreasing the probability of quick, small course corrections.

In addition to defining the computations by which larvae navigate environments of varying light or varying odor, we also developed a quantitative model of odor-light integration. Previously, it has proven difficult to establish even a qualitative understanding of odor and light integration using static combinations of the two cues. Consider a simple experiment where a petri dish is divided into light and dark halves and a droplet of attractive odor is placed on the lighted half. If a larva moves towards the odor at the expense of moving out of darkness, is this because the larva naturally places more importance on odor than light regardless of intensity, because the particular concentrations of odor and intensities of light in the experiment favor a move towards odor, or because behavior is variable and larvae often make idiosyncratic choices? In our reverse-correlation experiments, we presented hundreds of larvae with thousands of combinations of light and odor variation and were thus able to resolve these

ambiguities. We determined not just how larvae balance an overall attraction to odor and aversion to light, but how they combine transient odor and light signals to make individual navigational decisions.

## Conclusion

Here we demonstrated the power of reverse-correlation analysis of larvae's behavioral responses to white-noise visual and fictive olfactory stimuli to decode the computations underlying the *Drosophila* larva's navigation of natural environments. We showed that this analysis could be used to decode the rules by which the larva integrates signals from distinct sensory organs. Larvae appear to use a single linear combination of odor and light inputs to make all navigational decisions, suggesting these signals are combined at early stages of the navigational circuitry.

We used optogenetics to explore how *perturbations in the activities* of identified neurons are interpreted behaviorally. We expressed CsChrimson in specific neurons to relate patterns of activity in these neurons to decisions regulating the frequency, size, and direction of turns (**Fig 2**). Using model parameters extracted from reverse correlation experiments, we were able to predict how larvae would respond to novel perturbations of these neurons' activities (**Fig 2C**). We explored how activity in one particular neuron type modulated the larva's responses to a natural light stimulus (**Fig 3,5,6**) and predicted how the larva's natural response to blue light steps (**Fig 4-iii**) would be altered by simultaneous perturbation of this neuron (**Fig 4-iv,v**). In this work, we addressed sensory neurons, but our approach can be used generally to identify computations carried out on activities of interneurons, to determine whether activity in a neuron is interpreted as attractive or aversive, to measure how that activity combines with other sources of information to produce decisions, and to find neurons most responsible for making navigational decisions (Koulakov et al., 2005).

## 338 **Materials and Methods**

### 339 **Fly strains**

340 The following strains were used: Canton-S and Berlin wild type (gift of Justin Blau), *w<sup>1118</sup>*;;20XUAS-  
341 *CsChrimson-mVenus* (Bloomington Stock #55136, gift of Vivek Jayaraman and Julie Simpson, Janelia  
342 Research Campus), *w\**;;*Gr21a-Gal4* (Bloomington stock #23890), *w\**;;*Or42a-Gal4* (Bloomington stock  
343 #9969), *w\**;;*Or42b-Gal4* (Bloomington stock #9972), *GMR-hid/CyO,P{sevRas1.V12}* (Bloomington stock  
344 #5771)

### 345 **Crosses:**

346 40 virgin female *UAS-CsChrimson* flies were crossed with 20 males of the selected Gal4 line. F1 progeny  
347 of both sexes were used for experiments.

### 348 **Larva Collection**

349 Flies were placed in 60mm embryo-collection cages (59-100 , Genessee Scientific) and allowed to lay  
350 eggs for 3 hours at 25C on enriched food media ("Nutri-Fly German Food," Genessee Scientific). For all  
351 experiments except the Berlin response to blue light (**Fig 2, top row and Fig 2 – figure supplement 1,**  
352 **top row**), the food was supplemented with 0.1 mM all-trans-retinal (ATR, Sigma Aldrich R2500), and  
353 cages were kept in the dark during egg laying. When eggs were not being collected for experiments, flies  
354 were kept either on plain food or agar (neither containing ATR).

355 Petri dishes containing eggs and larvae were kept at 25C (ATR+ plates were wrapped in foil) for 48-60  
356 hours. Second instar larvae were separated from the food using 30% sucrose solution and washed in  
357 deionized water. Larval stage was verified by size and spiracle morphology. Preparations for  
358 experiments were carried out in a dark room, under dim red (for phototaxis experiments) or blue (for



CsChrimson experiments) illumination. Prior to beginning experiments, larvae were dark adapted on a clean 2.5% agar surface for a minimum of 10 minutes.

## **Behavioral Experiments**

Approximately 30-50 larvae were transferred with a wet paintbrush to a 23cm square dish (Corning BioAssay Dish #431111), containing 2.5% (w/v) bacteriological grade agar (Apex, cat#20-274) and 0.75% (w/v) activated charcoal (DARCO G-60). The charcoal darkened the agar and improved contrast in our dark-field imaging setup. The plate was placed in a darkened enclosure and larvae were observed under strobed 850nm infrared illumination (Smartvision ODL-300-850) using a 14 fps 5 MP rolling shutter CMOS camera (Basler acA2500-14gm) in global-reset-release mode and an 18mm c-mount lens (Edmund Optics 54-857) equipped with an IR-pass filter (Hoya R-72). The experiments of Figure 3-3(b) were recorded using a 4MP global shutter CMOS camera (Basler acA2040-90umNIR) operating at 20 fps and a 35mm focal length lens (Fujinon CF35HA-1). A microcontroller (Teensy++ 2.0, PJRC) coordinated the infrared strobe and control of the stimulus light source, so stimulus presentation and images could be aligned to within the width of the strobe window (2-5 ms). Videos were recorded using custom software written in LABVIEW and analyzed using the MAGAT analyzer software package (Gershow et al., 2012). Further analysis was carried out using custom MATLAB scripts. Software is available at <https://github.com/GershowLab>

## **Stimulus Light Source**

We built a custom circuit board (Advanced Circuits, Colorado) containing 66 deep red high brightness LEDs (Philips Lumileds, LXM3-PD01, 655 nm central wavelength) and 12 royal blue high brightness LEDs (LXML-PR01-0500, 447.5 nm central wavelength) evenly distributed over ~25cm x 25cm. The LEDs were driven at constant current by a switch-mode LED driver circuit (based on LT3518, linear technology) operating at a switching frequency of 2 MHz. The on-current was set by interchangeable feedback

resistors and could be modulated separately for red and blue LEDs. The intensity of the red and blue LEDs was controlled separately by pulse-width-modulation. Illumination was provided from above the larvae; the LED circuit board was at the same height as the recording camera (~50 cm above the behavioral arena).

For multi-sensory experiments, the maximum red light intensity ( $911 \mu\text{W}/\text{cm}^2$ ) was 300 times greater than the maximum blue light intensity ( $3 \mu\text{W}/\text{cm}^2$ ). CsChrimson is slightly more sensitive to 655 nm than 448 nm light, so the blue light signal perturbed olfactory receptor neuron activity by less than 0.3% of the red-light signal's perturbation.

We calibrated the optical power of the LEDs using a photodiode power meter (S121C, Thorlabs, New Jersey) set to the central wavelength of the LEDs. We measured the uniformity of the stimulus light sources by imaging a Lambertian projector screen (Dalite 41466, Cousin's Video, Ohio) placed in the plane of the experimental arena under stimulus LED illumination.

### **Stimulus Sequences**

Stimulus protocols were generated with MATLAB and stored on an SD card for use by the microcontroller. Light intensity was modulated using pulse-width-modulation with a frequency of ~112 Hz (constrained to update exactly 8 times per camera frame).

### **Brownian Light Intensity**

We chose a Brownian random walk, whose derivatives on all time scales are independent identically distributed Gaussian variables, to analyze the larva's response to derivatives of stimulus intensity. Light levels were specified by values between 0 (off) and 255 (maximum intensity). Sequences of light levels corresponding to a random walk with reflecting boundary conditions were generated according to these rules:

$$I_0 = 127$$

$$I_j = -I_j \text{ if } I_j < 0$$

$$I_j = 510 - I_j \text{ if } I_j > 255$$

$$I_{j+1} = I_j + N(0, \sigma)$$

404 where  $N(0, \sigma)$  was a Gaussian random variable with mean 0 and variance  $\sigma^2$ . For the experiments  
 405 described in this work  $\sigma = 3$ . At an update rate of 112 Hz, this represents a diffusion constant of 504  
 406 (light levels)<sup>2</sup>/s. After the sequence of light levels was generated, the levels were rounded to the nearest  
 407 integer value before being transferred to the microcontroller for use in experiments. Sequences were  
 408 not reused within an experimental group but might be reused between groups. For multi-modal  
 409 experiments, independent sequences were used for each stimulus.

#### 410 **Step Responses**

411 For step response experiments of Figure 2C, a square wave with a period of 20 seconds and duty cycle  
 412 50% (10s high, 10 low) was presented. The low and high intensities were symmetrically distributed  
 413 about the mean light intensity of the reverse-correlation experiments.

414 For coordinated step response experiments of Figure 4, we presented steps of red and blue light  
 415 intensity. Every 10 seconds, each signal either increased from low to high, decreased from high to low,  
 416 or remained constant. The sequence of steps was chosen so that all combinations (except for both levels  
 417 remaining constant) were presented. For each stimulus, the low and high intensities were symmetrically  
 418 distributed about the mean light intensity of the reverse-correlation experiments.

#### 419 **Data Analysis**

420 As described previously (Gershow et al., 2012; Kane et al., 2013), videos of behaving larvae were  
 421 recorded using LabView software into a compressed image format (mmf) that discards the stationary

background. These videos were processed using computer vision software (written in C++ using the openCV library) to find the position and posture (head, tail, midpoint, and midline) of each larva and to assemble these into tracks, each following the movement of a single larva through time. These tracks were analyzed by Matlab software to identify behaviors, especially runs, turns, and head sweeps.

The sequence of light intensities presented to the larvae was stored with the video recordings and used for reverse correlation analysis.

### **Reverse Correlation Analysis**

**Turn-Triggered Averages** (Figure 2A, 3A, 5A) with a bin size of 0.1 second were computed by averaging stimulus values at the corresponding times relative to the start of a turn; e.g. the TTA at -1 second represents the average value of the derivative of the light intensity at all times that were between -.95 and -1.05 seconds before the initiation of a turn. The TTA at +1 second represents the same average for times 0.95 to 1.05 seconds after the initiation of a turn. We computed the TTA at positive times as a control – we expected the average to be nearly 0 at positive times because behavior is causal (decisions contain no information about the future stimulus). Due to the reflecting boundary conditions, on long time scales, derivatives of the stimulus were anti-correlated; thus the TTA is not exactly 0 at positive times.

**Convolution kernels:** We smoothed the TTA by fitting it to the impulse response of a third order linear system used to describe the calcium dynamics of *C. elegans* olfactory neurons (Kato 2013). This fit was used only to smooth the TTA; we do not ascribe any biological significance to the fit parameters. The smoothed kernel is shown as a black line in Fig 2A.

**Filtered stimulus:** We used the smoothed TTA as a convolution kernel to find the output of the linear filter stage of the LNP model. We scaled the kernel so that the variance of the filtered signal over the

entire stimulus history was 1. For the Canton-S red light experiments (Fig 2, second row), a kernel could not be recovered from the TTA, so the kernel for Gr21a>CsChrimson was used to calculate the turn-rate.

**Nonlinear Turn Rates:** (Fig 2B) The turn rate  $r(x_f)$  and standard error  $\sigma_r(x_f)$  as a function of filtered signal value  $x_f$  were computed by

$$r(x_f) = \frac{N_{turn}(x_f)}{N_{all}(x_f)} * \frac{1}{\Delta t}$$

$$\sigma_r(x_f) = \frac{\sqrt{N_{turn}(x_f)}}{N_{all}(x_f)} * \frac{1}{\Delta t}$$

$N_{turn}$  is the number of turns observed with the filtered signal within the histogram bin (size = 0.25) containing  $x_f$  and  $N_{all}$  is the total number of data points where the filtered signal was in the histogram bin and larvae were in runs and thus capable of initiating turns, and  $\Delta t$  was the sampling period (1/14 s).

By construction, the stimulus ensemble is Gaussian distributed with mean 0 and variance 1. If the turn-triggered ensemble is also Gaussian distributed, then the turn rate is given by a ratio-of-Gaussians (Pillow and Simoncelli, 2006)

$$r_{ROG}(x) = \bar{r} \frac{e^{-\frac{(x-\mu)^2}{2\sigma^2}}}{\sigma e^{-\frac{x^2}{2}}}; \bar{r} = \frac{N_{turn}}{T}; \mu = E[x_f | \text{turn}]; \sigma^2 = E[(x_f - \mu)^2 | \text{turn}]$$

$r_{ROG}(x)$  is plotted in Fig 2B as a black line. This rate function was used for the predictions in Fig 2C (cyan lines), with  $\bar{r}$ ,  $\sigma$ , and  $\mu$  calculated directly from the turn-triggered ensemble.

**Size-sorted TTAs** (Fig 2D, 5B) were computed in the same manner, but the analysis was conducted separately for turns where the resulting heading change (difference in headings between end of the previous and beginning of the next runs) was larger or smaller than the rms heading change for the population over the course of the experiments. The turn-size is determined by the size of the initial

head-sweep of the turn and by decisions made after turn-initiation (at positive times), so we did not expect the size-sorted TTA to be identically 0 at positive times.

**Head sweep Triggered Averages** (Fig 2E, 5C) As for the TTA, but the reference time (0) was chosen as the beginning of either rejected or accepted head sweeps. Because the decision to accept or reject a head sweep is made after the beginning of the head sweep, we expected that the average would be nonzero at positive times corresponding to the duration of a head sweep. To simplify interpretation of the resulting averages, we considered only the first head sweep of each turn.

### Maximum-likelihood estimation of turn-rate parameters

In Figs 3 and 4, we fit the nonlinear turn rate to the observed data using the ratio-of-Gaussians function with  $\bar{r}$ ,  $\sigma$ , and  $\mu$  as fit parameters. The probability of observing at least one turn in an interval  $\Delta t$  given an underlying turn rate  $r$  is  $1 - e^{-r\Delta t}$ ; in the limit of short  $\Delta t$ , this reduces to  $r\Delta t$ . The probability of not observing a turn is  $e^{-r\Delta t}$ . Therefore given a model of the turn rate, the probability of observing a particular experimental outcome is

$$\log(P(\text{data}|\text{model})) = \sum_{\text{turn}} \log(r(x)\Delta t) - \sum_{\text{no turn}} r(x)\Delta t$$

where  $x$  is the filtered signal,  $r(x)$  is the turn rate predicted by the model, and  $\Delta t$  is the sampling rate.

$\sum_{\text{no turn}}$  is the sum over all points when larvae were in runs and thus capable of initiating turns. We used the MATLAB function `fmincon` to find the parameters that maximized this log-likelihood.

For figures 3C and 4 (cyan line), the separate pathways model rate function was given by

$$r(x) = \bar{r}_O \frac{e^{-\frac{(x_O - \mu_O)^2}{2\sigma_O^2}}}{\sigma_O e^{-\frac{x^2}{2}}} + \bar{r}_L \frac{e^{-\frac{(x_L - \mu_L)^2}{2\sigma_L^2}}}{\sigma_L e^{-\frac{x^2}{2}}} \text{ with fit parameters } \bar{r}_O, \sigma_O, \mu_O, \bar{r}_L, \sigma_L, \text{ and } \mu_L$$

478 For figures 3D and 4 (magenta line), the early linear combination model rate function was given by

479 
$$r(x) = \bar{r} \frac{e^{-\frac{(u-\mu)^2}{2\sigma^2}}}{\sigma e^{-\frac{u^2}{2}}}; u = \cos(\theta) x_O + \sin(\theta) x_L \text{ with fit parameters } \bar{r}, \sigma, \mu, \text{ and } \theta$$

#### 480 **Kullback-Leibler Divergence**

481 We estimated the KL divergences in Figure 3 using the k-nearest neighbors algorithm (Wang et al., 2009)  
 482 as implemented in MATLAB by (Szabó, 2014). As a check, for Figure 3B, we also analytically computed  
 483 the KL divergence between Gaussian distributions with the same means and (co-)variances as the  
 484 sampled turn-triggered and stimulus ensembles (Pillow and Simoncelli, 2006), and for Figure 3C,D, we  
 485 numerically calculated the KL divergence between the model predictions and a multivariate Gaussian  
 486 with the same mean and covariance as the measured turn-triggered density. For the univariate  
 487 distributions of 3B, we also estimated the divergence using an alternate method based on Szegő's  
 488 theorem (Ramirez et al., 2009) as implemented by (Szabó, 2014). None of the conclusions of this paper  
 489 depend on the method of estimation used.

KL divergence	k-NN	model data as normally distributed	Szegő-PSD method
Fig 3B: $D_{KL}(P(x_O, x_L   \text{turn})    P(x_O, x_L))$	.351	.325	
Fig 3B: $D_{KL}(P(x_O   \text{turn})    P(x_O))$	.236	.223	.235
Fig 3B: $D_{KL}(P(x_L   \text{turn})    P(x_L))$	.103	.100	.104
Fig 3B: $D_{KL}(P(u   \text{turn})    P(u))$	.334	.324	.333
Fig 3B: $D_{KL}(P(v   \text{turn})    P(v))$	.006	.0002	.003
Fig 3C: $D_{KL}(\text{data}    \text{model})$	.062	.035	
Fig 3D: $D_{KL}(\text{data}    \text{model})$	.030	.007	

490

491   **Acknowledgements:** We thank S. Nathasha Egodage and Ruben Contreras for assistance with  
492   experiments, and Damon Clark, Katherine Nagel, and Andrew Leifer for valuable comments on the  
493   manuscript



## REFERENCES

- 494 Albrecht, D.R., and Bargmann, C.I. (2011). High-content behavioral analysis of *Caenorhabditis elegans* in  
495 precise spatiotemporal chemical environments. *Nat Meth* 8, 599-605.
- 496 Angelaki, D.E., Gu, Y., and DeAngelis, G.C. (2009). Multisensory integration: psychophysics,  
497 neurophysiology, and computation. *Curr Opin Neurobiol* 19, 452-458.
- 498 Asahina, K., Louis, M., Piccinotti, S., and Vosshall, L.B. (2009). A circuit supporting concentration-  
499 invariant odor perception in *Drosophila*. *Journal of Biology* 8, 9.
- 500 Berg, H.C., and Brown, D.A. (1972). Chemotaxis in *Escherichia coli* analysed by Three-dimensional  
501 Tracking. *Nature* 239, 500-504.
- 502 Bialek, W., and van Steveninck, R.R. (2005). Features and dimensions: Motion estimation in fly vision.  
503 arXiv preprint q-bio/0505003.
- 504 Bretscher, Andrew J., Kodama-Namba, E., Busch, Karl E., Murphy, Robin J., Soltesz, Z., Laurent, P., and  
505 de Bono, M. (2011). Temperature, Oxygen, and Salt-Sensing Neurons in *C. elegans* Are Carbon Dioxide  
506 Sensors that Control Avoidance Behavior. *Neuron* 69, 1099-1113.
- 507 Busch, K.E., Laurent, P., Soltesz, Z., Murphy, R.J., Faivre, O., Hedwig, B., Thomas, M., Smith, H.L., and de  
508 Bono, M. (2012). Tonic signaling from O2 sensors sets neural circuit activity and behavioral state. *Nat*  
509 *Neurosci* 15, 581-591.
- 510 Busto, M., Iyengar, B., and Campos, A.R. (1999). Genetic dissection of behavior: modulation of  
511 locomotion by light in the *Drosophila melanogaster* larva requires genetically distinct visual system  
512 functions. *The Journal of neuroscience : the official journal of the Society for Neuroscience* 19, 3337-  
513 3344.
- 514 Chichilnisky, E.J. (2001). A simple white noise analysis of neuronal light responses. *Network-*  
515 *Computation in Neural Systems* 12, 199-213.
- 516 Chronis, N., Zimmer, M., and Bargmann, C.I. (2007). Microfluidics for in vivo imaging of neuronal and  
517 behavioral activity in *Caenorhabditis elegans*. *Nat Meth* 4, 727-731.
- 518 Clark, Damon A., Freifeld, L., and Clandinin, Thomas R. (2013). Mapping and Cracking Sensorimotor  
519 Circuits in Genetic Model Organisms. *Neuron* 78, 583-595.
- 520 Clark, D.A., Gabel, C.V., Gabel, H., and Samuel, A.D.T. (2007). Temporal Activity Patterns in  
521 Thermosensory Neurons of Freely Moving *Caenorhabditis elegans* Encode Spatial Thermal Gradients.  
522 *Journal of Neuroscience* 27, 6083-6090.

523 Dayan, P. (2001). Theoretical neuroscience: computational and mathematical modeling of neural  
524 systems (Cambridge, Mass: Massachusetts Institute of Technology Press).

525 Emonet, T., and Cluzel, P. (2008). Relationship between cellular response and behavioral variability in  
526 bacterial chemotaxis. *Proceedings of the National Academy of Sciences* 105, 3304-3309.

527 Faucher, C. (2006). Behavioral responses of *Drosophila* to biogenic levels of carbon dioxide depend on  
528 life-stage, sex and olfactory context. *J Exp Biol* 209, 2739-2748.

529 Fishilevich, E., Domingos, A.I., Asahina, K., Naef, F., Vosshall, L.B., and Louis, M. (2005). Chemotaxis  
530 Behavior Mediated by Single Larval Olfactory Neurons in *Drosophila*. *Current Biology* 15, 2086-2096.

531 Frye, M.A., and Dickinson, M.H. (2004). Motor output reflects the linear superposition of visual and  
532 olfactory inputs in *Drosophila*. *J Exp Biol* 207, 123-131.

533 Gershow, M., Berck, M., Mathew, D., Luo, L., Kane, E.A., Carlson, J.R., and Samuel, A.D.T. (2012).  
534 Controlling airborne cues to study small animal navigation. *Nat Meth* 9, 290-296.

535 Gomez-Marin, A., and Louis, M. (2014). Multilevel control of run orientation in *Drosophila* larval  
536 chemotaxis. *Frontiers in Behavioral Neuroscience* 8.

537 Gomez-Marin, A., Stephens, G.J., and Louis, M. (2011). Active sampling and decision making in  
538 *Drosophila* chemotaxis. *Nat Commun* 2, 441.

539 Hassan, J., Iyengar, B., Scantlebury, N., Rodriguez Moncalvo, V., and Campos, A.R. (2005). Photic input  
540 pathways that mediate the *Drosophila* larval response to light and circadian rhythmicity are  
541 developmentally related but functionally distinct. *The Journal of Comparative Neurology* 481, 266-275.

542 Heckscher, E.S., Lockery, S.R., and Doe, C.Q. (2012). Characterization of *Drosophila* Larval Crawling at the  
543 Level of Organism, Segment, and Somatic Body Wall Musculature. *J Neurosci* 32, 12460-12471.

544 Jones, W.D., Cayirlioglu, P., Grunwald Kadow, I., and Vosshall, L.B. (2007). Two chemosensory receptors  
545 together mediate carbon dioxide detection in *Drosophila*. *Nature* 445, 86-90.

546 Kane, E.A., Gershow, M., Afonso, B., Larderet, I., Klein, M., Carter, A.R., de Bivort, B.L., Sprecher, S.G.,  
547 and Samuel, A.D. (2013). Sensorimotor structure of *Drosophila* larva phototaxis. *Proc Natl Acad Sci U S A*  
548 110, E3868-3877.

549 Kato, S., Xu, Y., Cho, Christine E., Abbott, L.F., and Bargmann, Cornelia I. (2014). Temporal Responses of  
550 *C. elegans* Chemosensory Neurons Are Preserved in Behavioral Dynamics. *Neuron* 81, 616-628.

551 Keene, A.C., Mazzoni, E.O., Zhen, J., Younger, M.A., Yamaguchi, S., Blau, J., Desplan, C., and Sprecher,  
552 S.G. (2011). Distinct Visual Pathways Mediate *Drosophila* Larval Light Avoidance and Circadian Clock  
553 Entrainment. *Journal of Neuroscience* 31, 6527-6534.

554 Keene, A.C., and Sprecher, S.G. (2012). Seeing the light: photobehavior in fruit fly larvae. *Trends in*  
555 *Neurosciences* 35, 104-110.

556 Kim, A.J., Lazar, A.A., and Slutskiy, Y.B. (2011). System identification of *Drosophila* olfactory sensory  
557 neurons. *J Comput Neurosci* 30, 143-161.

558 Klapoetke, N.C., Murata, Y., Kim, S.S., Pulver, S.R., Birdsey-Benson, A., Cho, Y.K., Morimoto, T.K., Chuong,  
559 A.S., Carpenter, E.J., Tian, Z., *et al.* (2014). Independent optical excitation of distinct neural populations.  
560 *Nat Meth* 11, 338-346.

561 Klein, M., Afonso, B., Vonner, A.J., Hernandez-Nunez, L., Berck, M., Tabone, C.J., Kane, E.A., Pieribone,  
562 V.A., Nitabach, M.N., Cardona, A., *et al.* (2014). Sensory determinants of behavioral dynamics  
563 in *Drosophilathermotaxis*. *Proceedings of the National Academy of Sciences*, 201416212.

564 Korobkova, E., Emonet, T., Vilar, J.M.G., Shimizu, T.S., and Cluzel, P. (2004). From molecular noise to  
565 behavioural variability in a single bacterium. *Nature* 428, 574-578.

566 Koulakov, A.A., Rinberg, D.A., and Tsigankov, D.N. (2005). How to Find Decision Makers in Neural  
567 Networks. *Biological Cybernetics* 93, 447-462.

568 Kreher, S.A., Kwon, J.Y., and Carlson, J.R. (2005). The Molecular Basis of Odor Coding in the *Drosophila*  
569 Larva. *Neuron* 46, 445-456.

570 Kreher, S.A., Mathew, D., Kim, J., and Carlson, J.R. (2008). Translation of Sensory Input into Behavioral  
571 Output via an Olfactory System. *Neuron* 59, 110-124.

572 Kwon, J.Y., Dahanukar, A., Weiss, L.A., and Carlson, J.R. (2007). The molecular basis of CO<sub>2</sub> reception in  
573 *Drosophila*. *Proceedings of the National Academy of Sciences* 104, 3574-3578.

574 Lahiri, S., Shen, K., Klein, M., Tang, A., Kane, E., Gershow, M., Garrity, P., and Samuel, A.D.T. (2011). Two  
575 Alternating Motor Programs Drive Navigation in *Drosophila* Larva. *PLoS ONE* 6, e23180.

576 Lockery, S.R. (2011). The computational worm: spatial orientation and its neuronal basis in *C. elegans*.  
577 *Curr Opin Neurobiol* 21, 782-790.

578 Louis, M., Huber, T., Benton, R., Sakmar, T.P., and Vosshall, L.B. (2008). Bilateral olfactory sensory input  
579 enhances chemotaxis behavior. *Nat Neurosci* 11, 187-199.

580 Luo, L., Gabel, C.V., Ha, H.I., Zhang, Y., and Samuel, A.D.T. (2008). Olfactory behavior of swimming C-  
581 elegans analyzed by measuring motile responses to temporal variations of odorants. *Journal of*  
582 *Neurophysiology* 99, 2617-2625.

583 Luo, L., Gershow, M., Rosenzweig, M., Kang, K., Fang-Yen, C., Garrity, P.A., and Samuel, A.D.T. (2010).  
584 Navigational Decision Making in *Drosophila* Thermotaxis. *Journal of Neuroscience* 30, 4261-4272.

585 Luo, L., Wen, Q., Ren, J., Hendricks, M., Gershow, M., Qin, Y., Greenwood, J., Soucy, E.R., Klein, M.,  
586 Smith-Parker, H.K., *et al.* (2014). Dynamic Encoding of Perception, Memory, and Movement in a C.  
587 elegans Chemotaxis Circuit. *Neuron* 82, 1115-1128.

588 Ma, W.J., Beck, J.M., Latham, P.E., and Pouget, A. (2006). Bayesian inference with probabilistic  
589 population codes. *Nat Neurosci* 9, 1432-1438.

590 Miller, A.C., Thiele, T.R., Faumont, S., Moravec, M.L., and Lockery, S.R. (2005). Step-Response Analysis of  
591 Chemotaxis in *Caenorhabditis elegans*. *J Neurosci* 25, 3369-3378.

592 Monte, P., Woodard, C., Ayer, R., Lilly, M., Sun, H., and Carlson, J. (1989). Characterization of the larval  
593 olfactory response in *Drosophila* and its genetic basis. *Behavior genetics* 19, 267-283.

594 Olsen, S.R., and Wilson, R.I. (2008). Cracking neural circuits in a tiny brain: new approaches for  
595 understanding the neural circuitry of *Drosophila*. *Trends in Neurosciences* 31, 512-520.

596 Pierce-Shimomura, J.T., Morse, T.M., and Lockery, S.R. (1999). The fundamental role of pirouettes in  
597 *Caenorhabditis elegans* chemotaxis. *The Journal of Neuroscience: The Official Journal of the Society for*  
598 *Neuroscience* 19, 9557-9569.

599 Pillow, J.W., and Simoncelli, E.P. (2006). Dimensionality reduction in neural models: An information-  
600 theoretic generalization of spike-triggered average and covariance analysis. *Journal of Vision* 6, 414-428.

601 Python, F.o., and Stocker, R.F. (2002). Adult-like complexity of the larval antennal lobe of *D.*  
602 *melanogaster* despite markedly low numbers of odorant receptor neurons. *The Journal of Comparative*  
603 *Neurology* 445, 374-387.

604 Ramirez, D., Via, J., Santamaria, I., and Crespo, P. (2009). ENTROPY AND KULLBACK-LEIBLER DIVERGENCE  
605 ESTIMATION BASED ON SZEGO'S THEOREM.

606 Ringach, D., and Shapley, R. (2004). Reverse correlation in neurophysiology. *Cognitive Science* 28, 147-  
607 166.

608 Ryu, W.S., and Samuel, A.D.T. (2002). Thermotaxis in *Caenorhabditis elegans* analyzed by measuring  
609 responses to defined thermal stimuli. *Journal of Neuroscience* 22, 5727-5733.

610 Salcedo, E., Huber, A., Henrich, S., Chadwell, L.V., Chou, W.H., Paulsen, R., and Britt, S.G. (1999). Blue-  
611 and green-absorbing visual pigments of *Drosophila*: ectopic expression and physiological  
612 characterization of the R8 photoreceptor cell-specific Rh5 and Rh6 rhodopsins. *The Journal of*  
613 *neuroscience : the official journal of the Society for Neuroscience* 19, 10716-10726.

614 Sawin, F.P., Harris, L.R., Campos, A.R., and Sokolowski, M.B. (1994). Sensorimotor Transformation from  
615 Light Reception to Phototactic Behavior in *Drosophila* Larvae (Diptera, Drosophilidae). *Journal of Insect*  
616 *Behavior* 7, 553-567.

617 Scantlebury, N., Sajic, R., and Campos, A.R. (2007). Kinematic Analysis of *Drosophila* Larval Locomotion  
618 in Response to Intermittent Light Pulses. *Behavior Genetics* 37, 513-524.

619 Schwartz, O., Pillow, J.W., Rust, N.C., and Simoncelli, E.P. (2006). Spike-triggered neural characterization.  
620 *Journal of Vision* 6, 484-507.

621 Segall, J.E., Block, S.M., and Berg, H.C. (1986). TEMPORAL COMPARISONS IN BACTERIAL CHEMOTAXIS.  
622 *Proceedings of the National Academy of Sciences of the United States of America* 83, 8987-8991.

623 Shimizu, T.S., Tu, Y., and Berg, H.C. (2010). A modular gradient-sensing network for chemotaxis in  
624 *Escherichia coli* revealed by responses to time-varying stimuli. *Molecular Systems Biology* 6.

625 Sprecher, S.G., and Desplan, C. (2008). Switch of rhodopsin expression in terminally differentiated  
626 *Drosophila* sensory neurons. *Nature* 454, 533-537.

627 Suzuki, H., Thiele, T.R., Faumont, S., Ezcurra, M., Lockery, S.R., and Schafer, W.R. (2008). Functional  
628 asymmetry in *Caenorhabditis elegans* taste neurons and its computational role in chemotaxis. *Nature*  
629 454, 114-117.

630 Szabó, Z. (2014). Information Theoretical Estimators Toolbox. *Journal of Machine Learning Research* 15,  
631 283-287.

632 Wang, Q., Kulkarni, S.R., and Verdu, S. (2009). Divergence Estimation for Multidimensional Densities Via  
633 -Nearest-Neighbor Distances. *IEEE Transactions on Information Theory* 55, 2392-2405.

634 Westwick, D.T., Medicine, I.E.i., and Biology, S. (2003). Identification of nonlinear physiological systems  
635 ([Piscataway, N.J.?] : Hoboken, NJ: IEEE Press ; Wiley-Interscience).

636

637

**Figure 1: Identifying computations underlying the decision to initiate a turn. A Computation:** on the basis of sensory input (light or odor in this work) the larva decides whether or not to end a run and begin a turn. **B LNP model of the computation:** Sensory input is processed by a linear filter to produce an intermediate signal. The rate at which the larva initiates turns is a nonlinear function of this signal. Turns are initiated stochastically according to a Poisson process with this underlying turn rate. **C Reverse-Correlation to determine LNP parameters: 1.** Overview of the experiment. We presented groups larvae with either blue or red light with randomly varying intensity derivatives. Blue light provided a visual stimulus, while red light activated CsChrimson expressed in sensory neurons. In multi-sensory experiments, uncorrelated red light and blue light signals are presented simultaneously. Larvae are observed under infrared illumination, and their behaviors are analyzed with machine vision software. **2.** We calculate the “turn-triggered average” (TTA) or the reverse-correlation between turn-initiation and stimulus by averaging the stimulus that preceded each moment any larva initiated a turn. The TTA approximates the convolution kernel for the linear response of the LNP model. **3.** Calculate the inferred filtered signal. Using the TTA as a convolution kernel and the known input signal, we compute the intermediate filtered signal. **4.** Calculate the nonlinear rate function. Using the inferred filtered signal and the observed times at which turns were initiated, we find the nonlinear rate function by dividing the distribution of filtered signal values at the time of turn initiation (“turn-triggered-ensemble”) by the distribution of all filtered signal values. Illustrations adapted from (Kane,2013).

**Video 1: Calculating the turn-triggered average. Left panel:** annotated video image of individual larva. Thin white line: larva’s path (past and future). Gold dots: markers along midline of animal, used to determine posture. Upper left corner: time (since experiment start) and behavioral state. **Right panels:** top: light derivative (AU) vs. time; current time is indicated by dashed cyan line. Middle panels: speed and body bend angle, metrics used to determine behavioral state, vs. time. Shading indicates behavioral state (blue = run, white = turn; within turns, red = rejected head sweep, green = accepted head sweep). Current time is indicated by cyan dot. Bottom panel: turn-triggered average light intensity derivative (AU), calculated based on turns preceding the one shown.

**Animation:** The time preceding and following individual turns is featured. At the moment a larva initiates a turn, we “grab” the sequence of light intensity derivatives and add it to a running average (shown at the bottom). As we include more turns in the average (number of included turns is indicated by “turn #” above the left panel – note logarithmic spacing of turn #s), we build up a “turn-triggered-average” that approximates the linear filter in the LNP model.

**Figure 2: Unimodal Reverse-Correlation Experiments** Top row, Berlin wild type larvae were stimulated with blue ( $\lambda_{\text{peak}} = 448 \text{ nm}$ ; max intensity =  $74 \mu\text{W}/\text{cm}^2$ ) light. All other rows, larvae of indicated genotype were stimulated with red light ( $\lambda_{\text{peak}} = 655 \text{ nm}$ ; max intensity =  $911 \mu\text{W}/\text{cm}^2$ ) while constant dim blue light (intensity =  $3.7 \mu\text{W}/\text{cm}^2$ ) served as a visual mask. **Column A:** Turn triggered average. Average stimulus preceding (and following) each turn initiation. Turns are initiated at time 0 (indicated with dashed line). The black line is the smoothed TTA used as the linear filter. **Column B:** Measured turn-rates as a function of calculated filter output. Line and shaded region represent mean turn rate and standard error due to counting statistics. Black line is the nonlinear turn-rate modeled as a ratio-of-gaussians (Pillow 2006). **Column C: Step responses predicted by LNP model.** Square waves of light with period 20s and duty cycle 50% were presented to larvae. The LNP model was used to predict the resulting turn rates. Top graphs: light level vs. time in cycle. A favorable change happens at  $t = 0$  and an unfavorable change at  $t = 10\text{s}$ . Bottom graphs: measured and predicted turn rates vs. time in cycle. Black line and shaded region represent mean turn rate and standard error due to counting statistics. The cyan line is the exact prediction of the model using the parameters found from the corresponding reverse-correlation experiments (A,B). The stimulus and analysis were cyclic, so the time range from -2 to 0 seconds is identical to that from 18-20 seconds. **Column D: Size-sorted turn-triggered average.** As in A, but turns were sorted into large (heading change during turn > rms heading change) and small turns. Displayed averages are lowpassed with a Gaussian filter ( $\sigma = 0.5\text{s}$ ) to clarify the long time-scale features. **Column E** Head-sweep triggered average (for first head-sweep of turn). Average stimulus surrounding accepted (teal) and rejected (red) head-sweeps. Headsweeps were initiated at time  $t=0$  and concluded at a variable time in the future. The mean head-sweep duration (1.25s) is indicated by the shaded region

See table 1 for number of experiments, animals, etc.

**Figure 2 – figure supplement 1: LNP model parameters are stable for duration of 20 minute experiments.** Experiments of figure 2 analyzed separately using data only from the first 10 minutes of experiment (teal) or only from the second ten minutes of experiment (purple) or from entire 20 minute data set (black). **Column A: Turn triggered average.** As in 2A. The same convolution kernel is recovered from all three data sets. **Column B: Measured turn-rates as a function of calculated filter output.** As in 2B. The turn rates vary across the three data sets mainly at high values of the filter output (stimulus conditions most likely to lead to turning). **Column C: LNP model fits can predict response to white noise signals.** Data from the first ten minutes of the experiments were used to find LNP model parameters. The parameterized models were then used to predict the turn rate at each time point during the second 10 minutes of experiments. The measured turn rate during the second 10 minutes is plotted as a function of the model predictions. At high turn rates, for visual and fictive attractive odor stimuli, the turn rate is lower in the final 10 minutes than predicted by fits to the first 10 minutes, suggesting modest adaptation. For fictive  $\text{CO}_2$ , the measured turn rate is higher than predicted, suggesting modest sensitization. Error bars represent the uncertainty due to counting statistics.

**Figure 3: Multi-modal reverse-correlation experiments suggest attractive odor and light signals are combined linearly and early.** *Or42a>CsChrimson* larvae were presented with independently varying Brownian light intensities. Reverse-correlation analysis was carried out as in figure 1. **A Turn-triggered average.** Average change in red (fictive odor) and blue light intensities preceding turns. **B Turn triggered ensemble.** Top: 2D density histogram of calculated odor and light filter outputs at initiation of each turn. Bottom: 1D density histograms of filter outputs ( $x_O, x_L$ ) and their linear combinations ( $u, v$ ).  $D_{KL}(P(x | \text{turn}) || P(x))$  is the Kullback-Leibler divergence from the turn-triggered distribution to the distribution of  $x$  at all times. Larger values indicate that  $x$  carries more information about the decision to turn. **(C-D) Predicted turn triggered ensemble according to** (C) Independent pathways model and (D) Early linear combination model. Top panel: predicted density. Bottom panel: difference between predicted density and measured density.  $D_{KL}(\text{data} || \text{model})$  is the Kullback-Leibler divergence of the model from the data; smaller values indicate a better match. \*\*\*\*\* =  $P(\text{Independent pathways model}) / P(\text{Early linear combination model}) < 0.00001$ ; Aikake Information Criterion Test. **E** Coordinate rotation described in text and used in bottom panel of B. Orthogonal coordinates ( $u, v$ ) are rotated  $33^\circ$  relative to ( $x_O, x_L$ ). Rotation is shown overlaid on turn-triggered probability density (B).

See table 1 for number of experiments, animals, etc.

**Figure 3 – figure supplements 1 and 2:** Graphical explanations of the independent pathways and early linear combination models described in the text. We envision the titles of 3C and 3D being clickable links to these figures.

**Figure 3 – figure supplement 3: Visual and fictive olfactory stimuli do not cross-talk.** Larvae were presented with same red and blue Brownian light stimuli as in Figure 3. Turn-triggered average of red and blue stimuli are shown on same axes as in Figure 3A. **(a)** Reproduced from Figure 3A: Larvae expressing *CsChrimson* in *Or42a* receptor neurons turn in response to increasing blue light and decreasing red light (fictive odor). **(b)** Genetically blinded larvae expressing *CsChrimson* in *Or42a* receptor neurons turn in response to decreasing red light (fictive odor) but are unresponsive to blue light. **(c)** Wild type larvae not expressing *CsChrimson* turn in response to increasing blue light but are unresponsive to red light. See table 1 for number of experiments, animals, etc.



**Figure 4 Multi-modal step responses support early linear combination of odor and light signals.** Turn rates vs. time for *Or42a>CsChrimson* larvae responding to coordinated increases and decreases of red and blue light. All steps occur at  $t = 0$ . Left column: no change in fictive odor, center column: red light increases at  $t = 0$  right column: red light decreases at  $t = 0$ . Top row: no change in visual stimulus, center row: blue light increases at  $t = 0$ , bottom row: blue light decreases at  $t = 0$ . For instance, in panel **iii** blue light increased at time 0, while red light remained constant; in **iv**, both red and blue light increased at time 0; and in **v**, blue light increased and red light decreased at time 0.

Black line and shaded region represent mean turn rate and standard error due to counting statistics. Teal line is the best-fit (maximum likelihood estimate, 6 parameter fit) prediction of the independent pathways model. Magenta line is the best-fit (maximum likelihood estimate, 4 parameter fit) prediction of the early linear combination model. Note that the time-axis is the same for each subplot, but the turn-rate axis varies. \*\*\*\*\* =  $P(\text{Independent pathways model}) / P(\text{Early linear combination model}) < 0.00001$ ; Aikake Information Criterion Test, measured for the entire data set. See table 1 for number of experiments, animals, etc.

**Figure 5 All navigational decisions appear to be based on a single linear combination of odor and light inputs. (A-C) Reverse correlation in rotated coordinate system.**  $\mu, \nu$  are linear combinations of the raw input stimuli according to the same scaling as used to combine filtered odor and light signals in Figure 3. **(A) Turn-triggered averages.** Average change in  $\mu, \nu$  prior to start of a turn. **B** Size-sorted turn-triggered averages. Displayed averages are lowpassed with a Gaussian filter ( $\sigma = 0.5s$ ) to clarify the long time-scale features. **C** Head-sweep-triggered average (for first head-sweep of turn). Shaded region indicates mean head-sweep duration (1.25 s).

**Figure 6 Probing for attentional shifts during multi-modal noise experiments.** **A** turn-triggered ensemble (duplicated from **Fig 3B**), with quadrants highlighted. Color scale the same as in 3B. Quadrants I-IV indicate which stimulus or stimuli likely provoked the larva to turn (I – both odor and light stimulated turning; II – Light, but not odor, stimulated turning; III – neither odor nor light were changing unfavorably; IV – Odor, but not light, stimulated turning). Each turn was assigned to one of these quadrants based on the filtered signal values ( $x_O$ ,  $x_L$ ) at the time the turn started. **(B,C) Difference in intensity changes during accepted and rejected headsweeps.** (first head-sweep of turn only) Difference in mean rate of change in intensity over mean headsweep duration (1.25s, shaded region in 5C) between rejected and accepted head-sweeps. Error bars are +/- 1 s.e.m. (B) Changes in odor and light intensities. (C) Changes in rotated coordinate system.

See table 1 for number of experiments, animals, etc.

Genotype	#expts	#animals	hours	#turns	rms turn size	#large turns	#small turns	#accepted head sweeps	#rejected head sweeps
Uni-modal Reverse-Correlation Experiments (Fig 2 A,B,D,E, 2-1)									
Berlin	6	150	52.6	6594	76.4	2462	4132	4139	2455
Canton-S	7	334	117.7	8824	66.0	3086	5738	5570	3254
Or42a>CsChrimson	5	180	61.1	6971	68.9	2531	4440	4122	2849
Or42b>CsChrimson	6	246	64.4	9565	73.3	3480	6085	6215	3350
Gr21a>CsChrimson	5	227	54.2	8760	75.1	3392	5368	5424	3336
Uni-modal Step Experiments (Fig 2 C)									
Berlin	4	95	34.7	3674					
Or42a>CsChrimson	2	107	36.6	3905					
Or42b>CsChrimson	2	99	21.5	2599					
Gr21a>CsChrimson	2	111	22.1	2384					
Multi-modal Reverse-Correlation Experiments (Fig 3,3-3,5,6)									
Or42a>CsChrimson	12	608	136	21075	66.6	7225	13850	12795	8280
quadrant I				10363				6216	4147
quadrant II				3301				2086	1215
quadrant III				1684				1088	596
quadrant IV				5727				3405	2322
GMR-Hid, Or42a>CsChrimson	3	121	28.9	4842					
Canton-S	3	166	39.9	3412					
Multi-modal Step Experiments (Fig 4)									
Or42a>CsChrimson	5	250	50	7859					

770

771 **Table 1: Numbers of experiments, animals, turns, and headsweeps for all figures.**

772 #expts: Number of 20 minute experiments. For reverse-correlation experiments, each experiment  
773 presented a different stimulus sequence with the same statistical properties; for step experiments, the  
774 same stimulus pattern was presented in each experiment.

775 #animals: Approximate number of animals, taken by finding the maximum number of animals tracked in  
776 a 30-second window during each experiment.

777 #hours: total observation time in units of larva-hours. Observing 3 larvae for 20 minutes each would  
778 equal 1 larva-hour.

779 #turns: total number of turns observed and used in analysis

780 rms turn size: root mean square turn size in degrees (defined as angular difference in run heading  
781 immediately before and after a turn) for the set of experiments

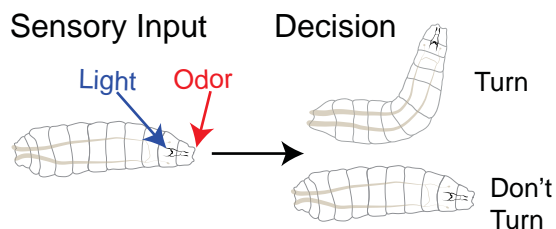
782 # large/small turns: number of turns with angular changes larger/smaller than the rms turn size

783 #accepted head sweeps: number of times the first head sweep of a turn was accepted, ending in a new  
784 run

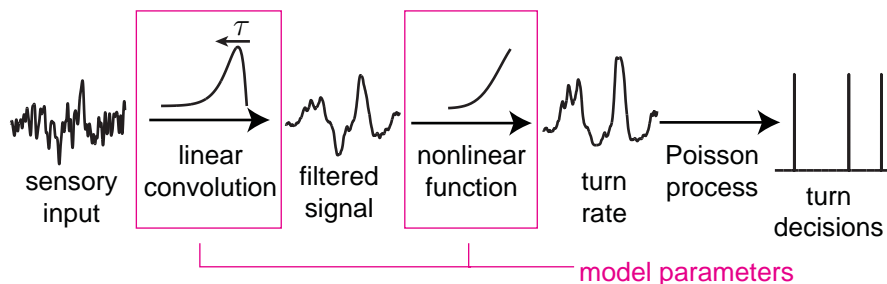
785 #rejected head sweeps: number of times the first head sweep of a turn was rejected, leading to another  
786 head sweep

**FIGURE 1**

## A Computation

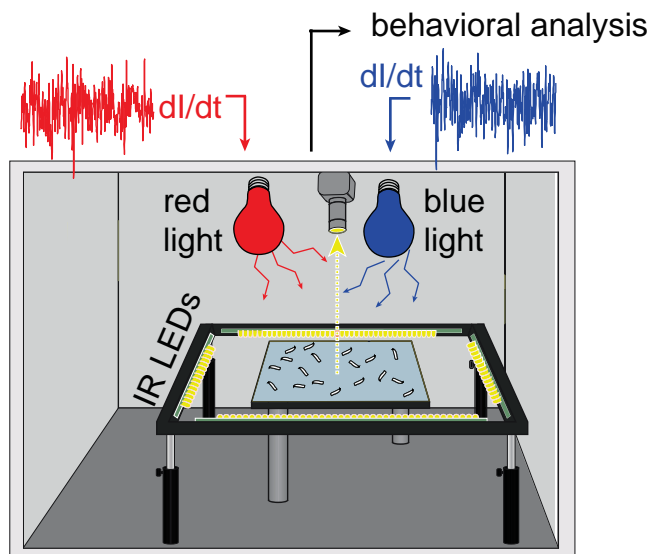


## B LNP Model

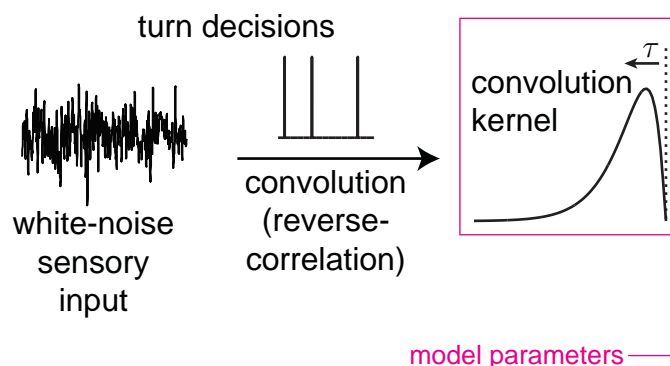


## C Reverse-Correlation to Determine LNP Model Parameters

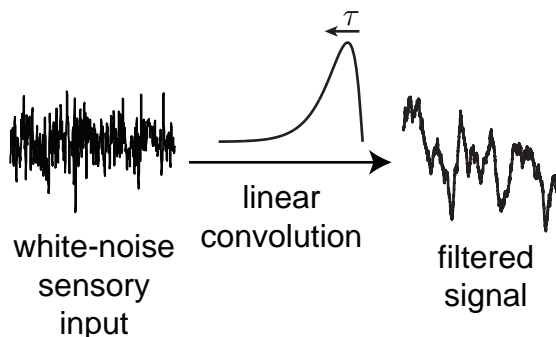
### 1. Record behavioral response to white-noise stimulus



### 2. Calculate turn-triggered average



### 3. Calculate filtered signal



### 4. Calculate nonlinear rate function

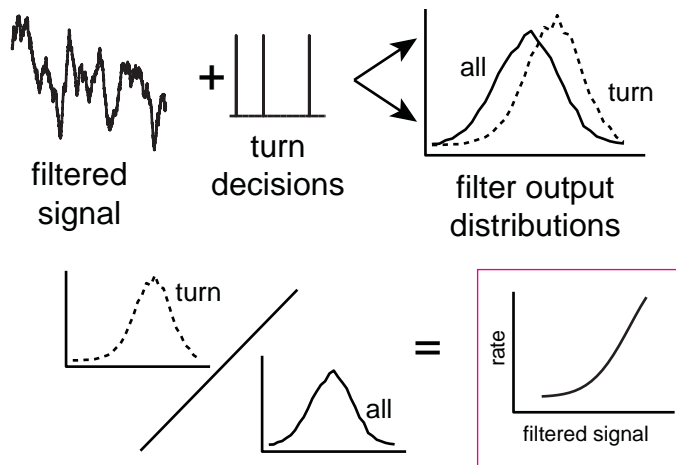


**FIGURE 2**

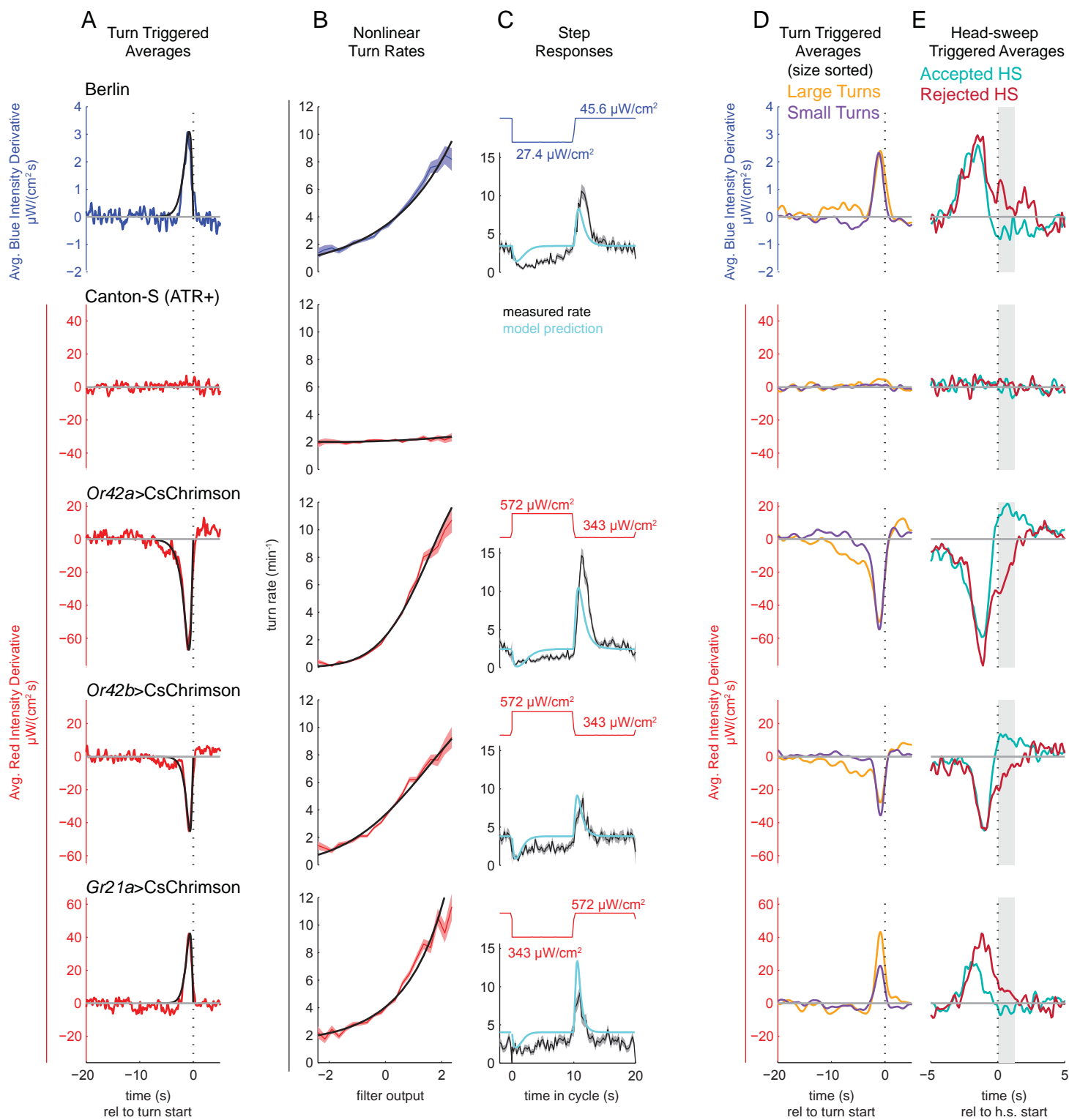


**FIGURE 3**

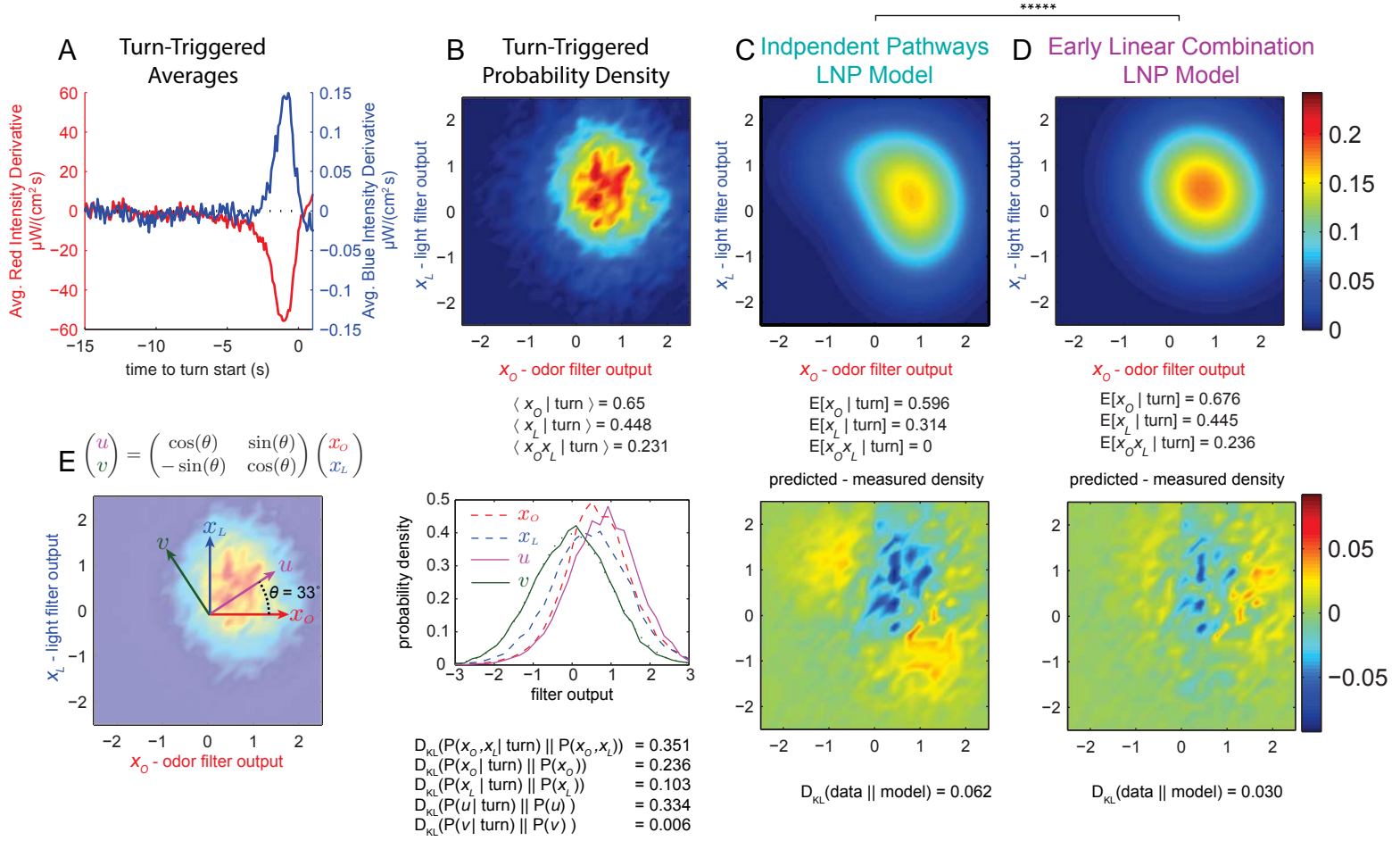


**FIGURE 4**

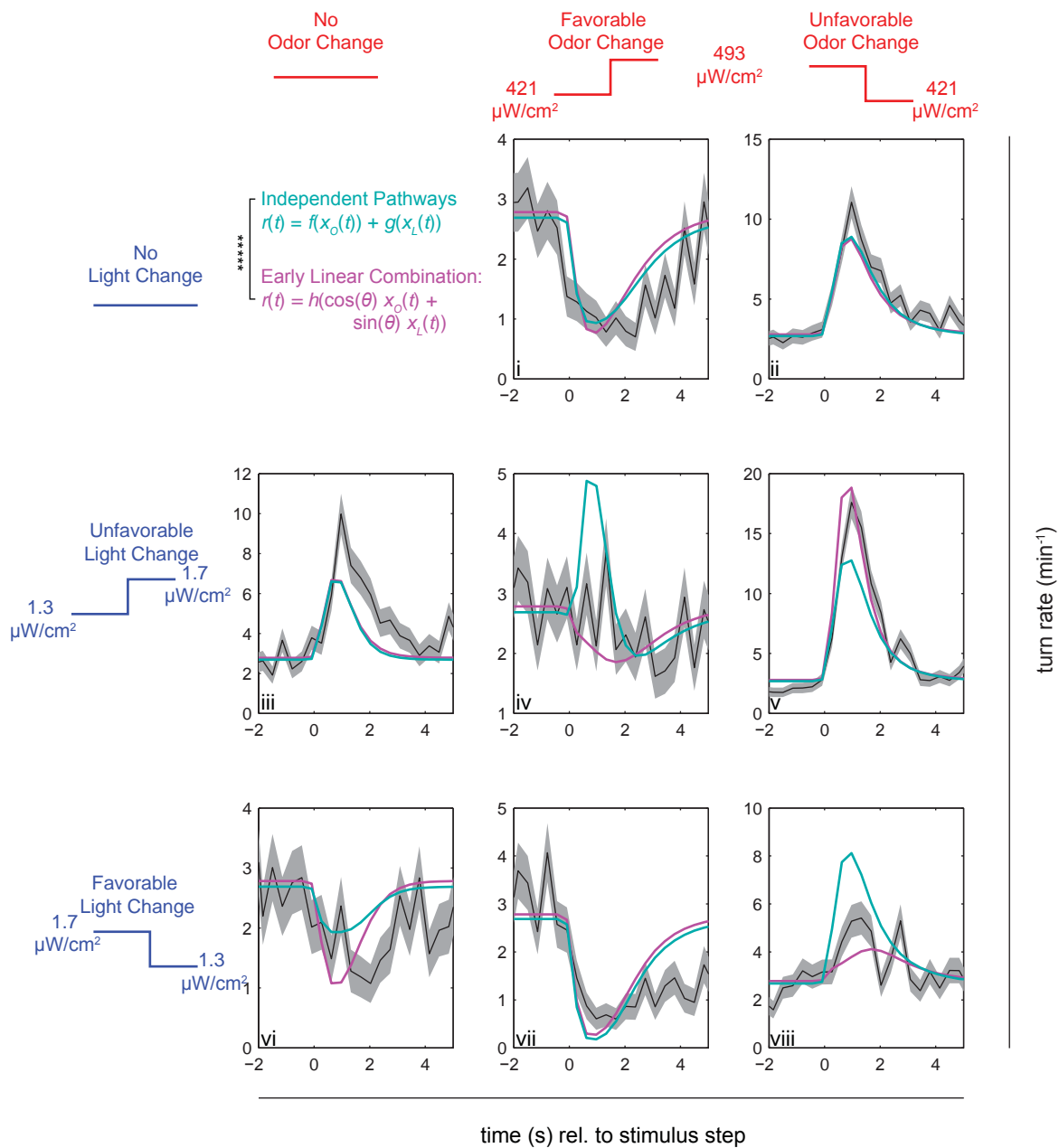
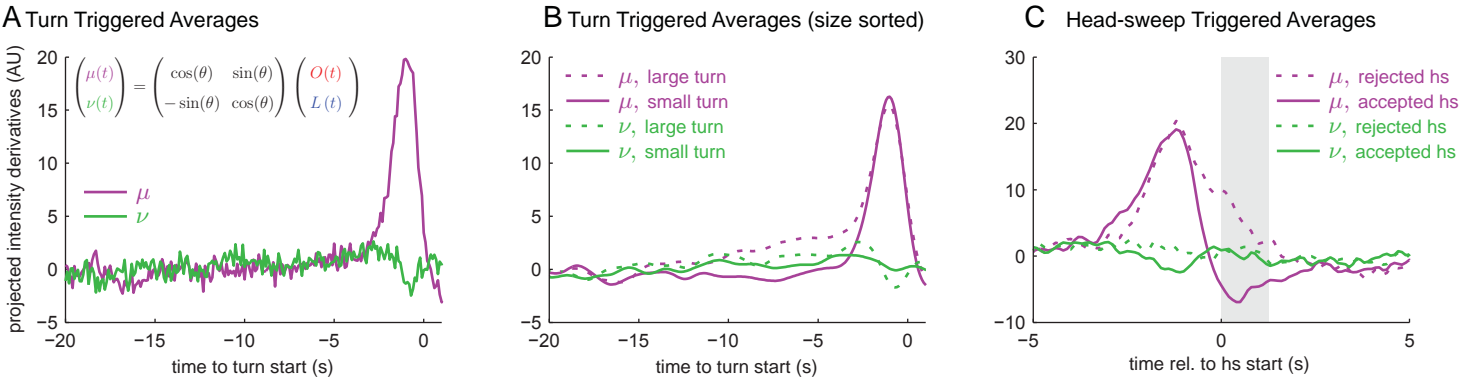




FIGURE 5



**FIGURE 6**

